Modelling Material Behavior

Ching-Chuan Huang

Professor Emeritus
Department of Civil Engineering,
National Cheng Kung University, Tainan, Taiwan
Email: samhcc@mail.ncku.edu.tw
2025/08/13

INTRODUCTION

This report series models the relationship between shear stress and shear displacement in soils using hyperbolic curves. The development and application of the hyperbolic soil model for various soil types are addressed in **Sections 10.1 through 10.5**. Section 10.6 explores models for porewater pressure driven by groundwater and seepage conditions. **Sections 10.7 to 10.9** examine three types of slope-facing systems that contribute to external support. Lastly, **Section 10.10** presents the theoretical framework for automatically generating noncircular failure mechanisms using logarithmic spirals.

10.1 MOHR-COULOMB FAILURE ENVELOPE

The Mohr-Coulomb failure envelope is known to exhibit curvature (see Fig. 10.1.1), indicating that the internal friction angle (φ) varies with the stress level. In other words, φ is stress-dependent and cannot be considered constant across different loading conditions:

$$\varphi = \tan^{-1}\left(\frac{\tau}{\sigma_n'}\right) \qquad (10-1-1)$$

τ: shear stress on the failure plane

σ_n': effective normal stress on the failure plane

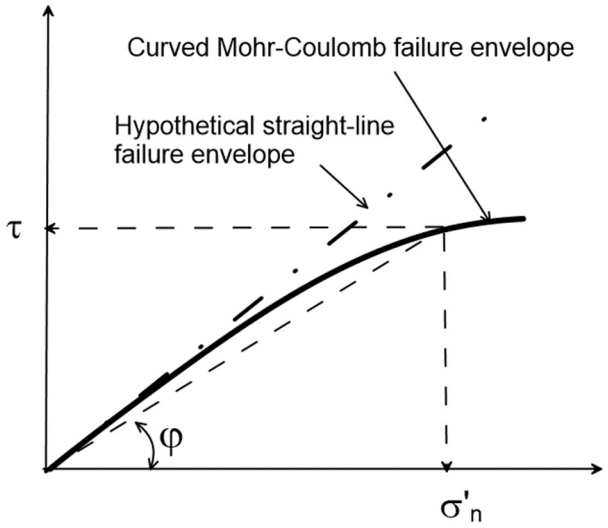

Figure 10.1.1 Curved Mohr-Coulomb failure envelope

For granular soils, a curved Mohr-Coulomb failure envelope is often represented

by the following empirical equation:

$$\varphi = \varphi_0 - \Delta\varphi \cdot \log\left(\frac{\sigma'_n}{\sigma'_r}\right) \qquad (10-1-2)$$

σ'_n: effective normal pressures

σ'_r: reference of effective normal pressure

The reference effective normal stress (σ'_r) defines the threshold beyond which the internal friction angle begins to decrease. Duncan and Wright (2005) summarized typical values for the peak friction angle (φ_o) and its reduction ($\Delta\varphi$) as functions of soil type, relative compaction (R.C.), and relative density (D_r). These relationships are presented in **Table 10.1.1**.

Table 10.1.2 provides values of cohesion c, φ_o, $\Delta\varphi$, σ'_r, and the maximum effective normal stress (σ'_{max}), derived from a series of direct shear tests conducted using medium to large shear boxes (compiled by Chiang, 2017). In this context, σ'_r corresponds to the minimum effective confining pressure (σ'_{min}) applied during testing. To clarify the applicability range of the data, σ'_{max} is also listed in the table as an upper bound reference. In practical applications, σ'_r is often substituted with atmospheric pressure (σ_{atm} = 101.3 kPa), following the recommendation by Duncan and Wright (2005).

Table 10.1.1 Summary of Mohr-Coulomb envelope based on $\sigma_r = \sigma_{atm}$ (101.3 kPa) suggested by Duncan and Wright (2005)

USCS(1)	R.C (%) .(2)	Dr (%) (3)	φ_0 (°)	$\Delta\varphi$ (°)
GW, SW	105	100	46	10
	100	75	43	8
	95	50	40	6
	90	25	37	4
GP, SP	105	100	42	9
	100	75	39	7
	95	50	36	5
	90	25	33	3
SM	100	-	36	8
	95	-	34	6
	90	-	32	4
	85	-	30	2

(1) USCS: Unified Soil Classification System; (2) R.C.: Relative Compaction; (3) Relative density

Table 10.1.2 Summary of Mohr-Coulomb envelope parameters obtained in some medium to large scale direct shear tests (Chiang, 2017)

Soil type, USCS[1] (Reference)	Direct share boxes dimensions (mm)	c (kPa)	φ_0 (°)	$\Delta\varphi$ (°)	σ_{min} *(kPa)*	σ_{max} *(kPa)*
Lin-Kou gravelly soil, GM (Chu et al., 1989)	1500*1500*750	0	49	0	47	305
San-Yi gravelly soil, GM (Chu et al., 1989)	1500*1500*750	0	58	*6.5*	75	130
Toyoura sand, SP (Qiu et al., 2000)	300*300*300	0	39	1.6	100	200
Gravelly lean clay, CL (Davoudi, 2011)	500×500×300	10	40	0	20	98
Chi-Chi sand, SW-SM (Wu, 2011)	90*90*50	0	49	7.8	56	217
Undisturbed clayey soil, CL (Huang, 2013)	300×300×200	6	25°	0	10	162
Mei-Shi sand, SP (Hsu, 2017)	300*300*250	0	40- 53	6.4- 12.0	20	100
Firouzkooh sand, SP (Ziaie Moayed et al., 2017)	300*300*154	0	36	0	109	218

(1) USCS: Unified Soil Classification System

10.2 HYPERBOLIC SOIL MODEL

The application of hyperbolic curves to simulate the stress–strain behavior of soils was first proposed by Duncan and Chang (1970). Building on this approach, Huang (2013) demonstrated that shear stress–shear displacement relationships observed in direct shear tests can also be effectively represented using hyperbolic models. The following hyperbolic equation, illustrated schematically in Fig. 10.1.1, characterizes the normalized shear stress (τ/τ_f) as a function of shear displacement (Δ) along a potential failure surface:

$$\frac{\tau}{\tau_f} = \frac{\Delta}{a + b \cdot \Delta} \qquad (10-2-1)$$

$$a = \frac{\tau_f}{k_{initial}} \qquad (10-2-2)$$

$$b = R_f \qquad (10-2-3)$$

$$R_f = \frac{\tau_f}{\tau_{ult}} \qquad (10-2-4)$$

$k_{initial}$: initial shear stiffness of soils

R_f: ratio between failure strength and asymptote ultimate shear strength

τ_{ult}: asymptote strength at infinite displacement

τ_f:: shear strength of soil based on Mohr-Coulomb failure criterion

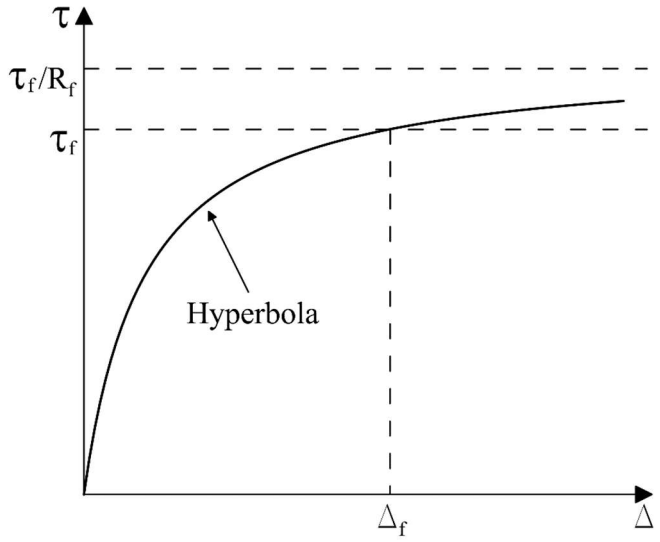

Figure 10.2.1 A hyperbolic shear stress vs. displacement relationship.

The shear strength of soils (τ_f) is defined by the Mohr-Coulomb failure criterion:

$$\tau_f = c + \sigma_n' \cdot \tan\varphi \qquad (10-2-5)$$

σ_n': Effective normal pressures

c: cohesion intercept

φ: Internal friction angle of soils

Note that Eq. (10-2-1) also represents the inverse of local safety factor F_s at the base of a slice (or a soil wedge):

$$F_s = \frac{\tau_f}{\tau} \qquad (10-2-6)$$

The initial shear stiffness can be expressed as a power function of effective normal stress (σ_n') acting on the failure surface:

$$k_{initial} = K \cdot G \left(\frac{\sigma'_n}{P_a} \right)^n \qquad (10-2-7)$$

K: shear stiffness number (a non-dimensional material constant)

P_a: atmospheric pressure (= 101.3 kPa)

G: reference shear stiffness (= 101.3 kPa/m)

n: exponent of stress dependency on soil stiffness

The hyperbolic stress–displacement relationship adopted here can be readily adapted to accommodate special cases, such as a linearly elastic pre-peak response followed by residual strength, or a hyperbolic pre-peak response followed by residual strength. The first scenario is a specific case of the second and can be simulated by setting **b = 0** in **Equation 10-2-1**, yielding:

$$\tau = \frac{\tau_f}{a} \cdot \Delta = k_{initial} \cdot \Delta \qquad (10-2-8)$$

10.3 HYPERBOLIC SOIL PARAMETERS

The results of hyperbolic curve fitting using shear stress–displacement data for various soils, obtained from medium- to large-scale direct shear tests, are summarized in **Tables 10.3.1 and Table 10.3.2**. Three key parameters of the hyperbolic model—namely, the stiffness number (K), the pressure dependency exponent (n), and the failure ratio (R_f)—have been curve-fitted for each test series reported in the table.

Figures 10.3.1 through 10.3.3 illustrate the fitted values of K, n, and R_f as functions of the internal friction angle (φ). Each figure includes upper and lower bounds to highlight the potential variability of these parameters. Notably, Figures 10.3.2 and **10.3.3** demonstrate that both K and n exhibit a positive correlation with φ, indicating that these values tend to increase as the internal friction angle increases. In contrast, the failure ratio R_f remains nearly constant throughout the entire range of φ investigated.

Table 10.3.1 Test conditions for some medium to large scale direct shear tests

Soil type, USCS[1] (Reference)	Direct share boxes dimensions Length*Width* Height (mm)	Specimen, D_r (%)[2]
Lin-Kou gravelly soil, GM (Chu et al., 1989)	1500*1500*750	In-situ
San-Yi gravelly soil, GM (Chu et al., 1989)	1500*1500*750	In-situ
Toyoura sand, SP (Qiu et al., 2000)	300*300*300	Re-molded, 90
Gravelly lean clay, CL (Davoudi, 2011)	500×500×300	In-situ
Chi-Chi sand, SW-SM (Wu, 2011)	90*90*50	Re-molded, 90
Undisturbed clayey soil, CL (Huang, 2013)	300×300×200	In-situ
Mei-Shi sand, SP (Hsu, 2017)	300*300*250	Re-molded, 29, 60, 87
Firouzkooh sand, SP (Ziaie Moayed et al., 2017)	300*300*154	Re-molded, 77

(1) USCS: Unified Soil Classification System

(2) Dr (%): Relative Density

Table 10.3.2 Test conditions of some medium to large scale direct shear tests and their hyperbolic parameters obtained in curve fitting

Soil type, USCS[1] (Reference)	c[1] (kPa)	φ[1] (°)	$\Delta\varphi$ (°)	K [2]	n [2]	R_f[2]
Lin-Kou gravelly soil, GM (Chu et al., 1989)	0	49	0	386	1.04	0.88
San-Yi gravelly soil, GM (Chu et al., 1989)	0	56-58	6.5	579	0.65	0.79
Toyoura sand, SP (Qiu et al., 2000)	0	38-39	1.6	400	0.025	0.43
Gravelly lean clay, CL (Davoudi, 2011)	10	40°	0	227	-0.5	0.78
Chi-Chi sand, SW-SM (Wu, 2011)	0	45-49	7.8	640	0.634	0.86
Undisturbed clayey soil, CL (Huang, 2013)	6	25°	0	87	0.15	0.74
Mei-Shi sand, SP (Hsu, 2017)	0	36- 53	6.4- 12.0	256- 664	0.3- 0.85	0.84- 0.87
Firouzkooh sand, SP (Moayed et al., 2017)	0	36	0	484	0.14	0.82

(1) Mohr-Coulomb failure envelope obtained at peak shear stress in direct shear tests

(2) Obtained from hyperbolic curve fitting based on shear stress- displacement data

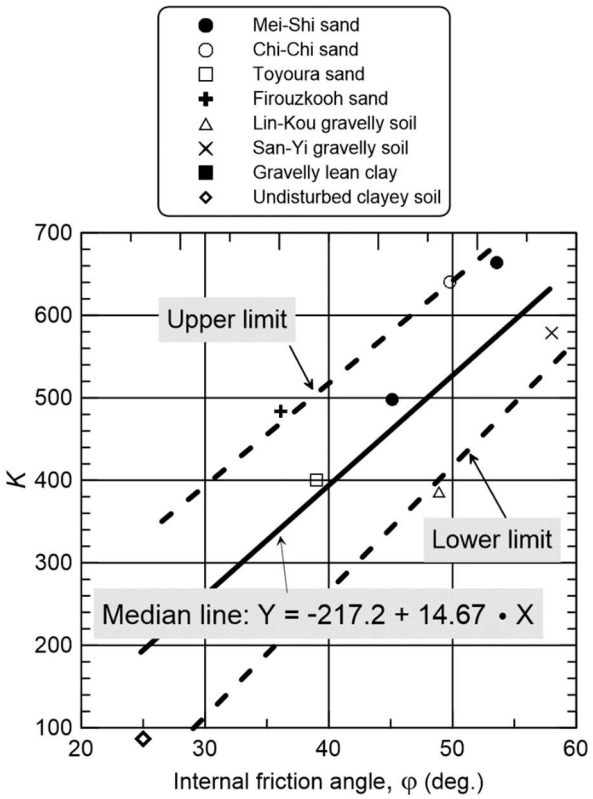

Figure 10.3.1 Curve-fitted parameter *K* for various types of soils

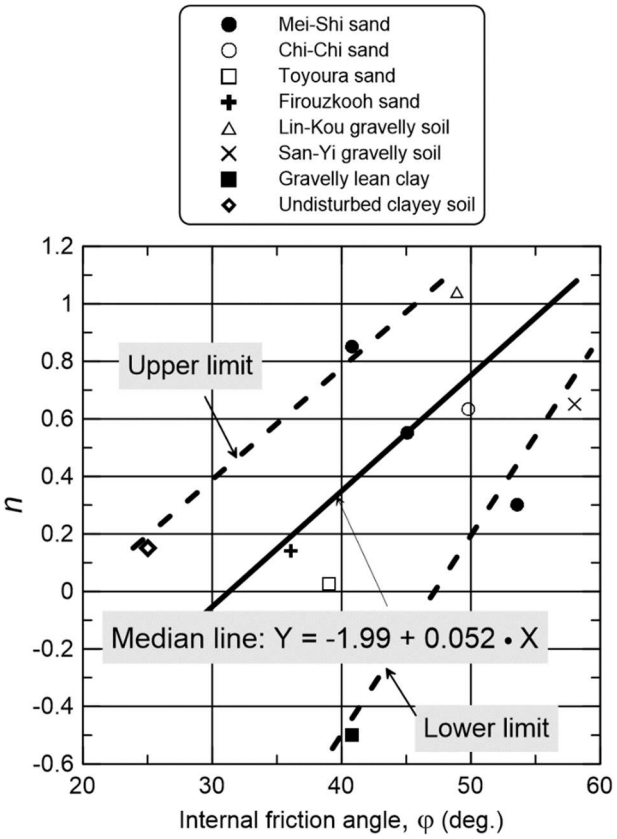

Figure 10.3.2 Curve-fitted parameter *n* for various types of soils

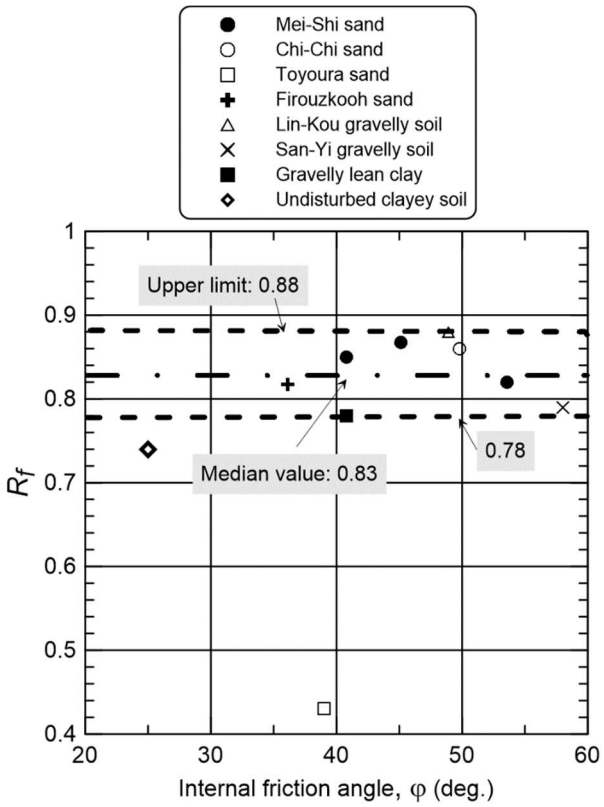

Figure 10.3.3 Curve-fitted parameter R_f for various types of soils

10.4 VALIDATION OF HYPERBOLIC PARAMETERS

To evaluate the effectiveness of the previously described shear stress–displacement model, representative parameters - taken from the median trend lines in **Figs. 10.3.1 to 10.3.3** and summarized in **Table 10.4.1** - are used to simulate shear stress–displacement behavior. Comparisons between experimental and simulated curves are presented in **Figs. 10.4.1 through 10.4.7**, covering seven test series reported by Chu (1989), Qiu et al. (2000), Davoudi (2011), Wu (2011), Hsu (2017), and Ziaie Moayed et al. (2017).

The model demonstrates good agreement with experimental results in capturing the pre-failure response of soils. However, for certain soil types, the post-failure behavior cannot be accurately reproduced using hyperbolic curves alone. A new soil model that incorporates post-failure characteristics is reported in **Series 11**.

Table 10.4.1 Soil parameters obtained from the median lines in Figs. 10.3.1- 10.3.3

Soil type, USCS (Reference)	K	n	R_f
Lin-Kou gravelly soil, GM (Chu et al., 1989)	500	0.7	0.83
San-Yi gravelly soil, GM (Chu et al., 1989)	620	1.0	0.83
Toyoura sand, SP (Qiu et al., 2000)	380	0.32	0.83
Gravelly lean clay, CL (Davoudi, 2011)	390	0.35	0.83
Chi-Chi sand, SW-SM (Wu, 2011)	640	0.634	0.83
Undisturbed clayey soil, CL (Huang, 2013)	200	-0.2	0.83
Mei-Shi sand, SP (Hsu, 2017)	580	0.9	0.83
Firouzkooh sand, SP (Ziaie Moayed et al., 2017)	360	0.15	0.83

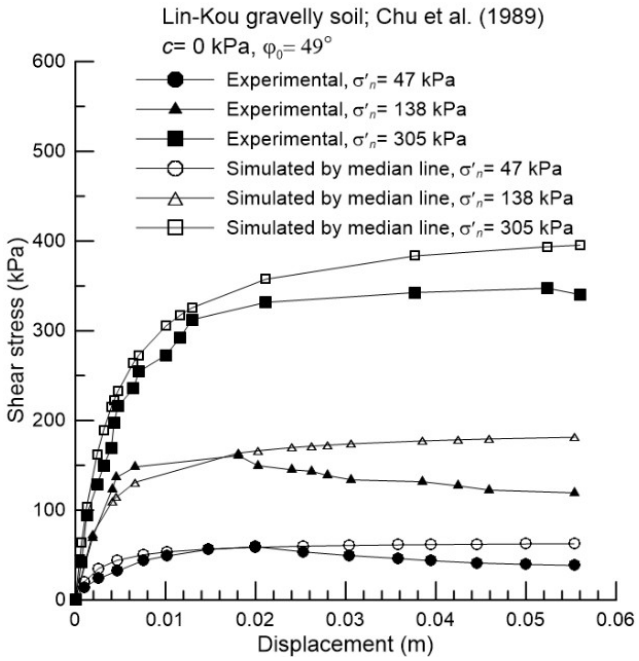

Figure 10.4.1 Comparisons of experimental and simulated stress-displacement curves for Lin-Kou gravelly soil reported by Chu et al. (1989)

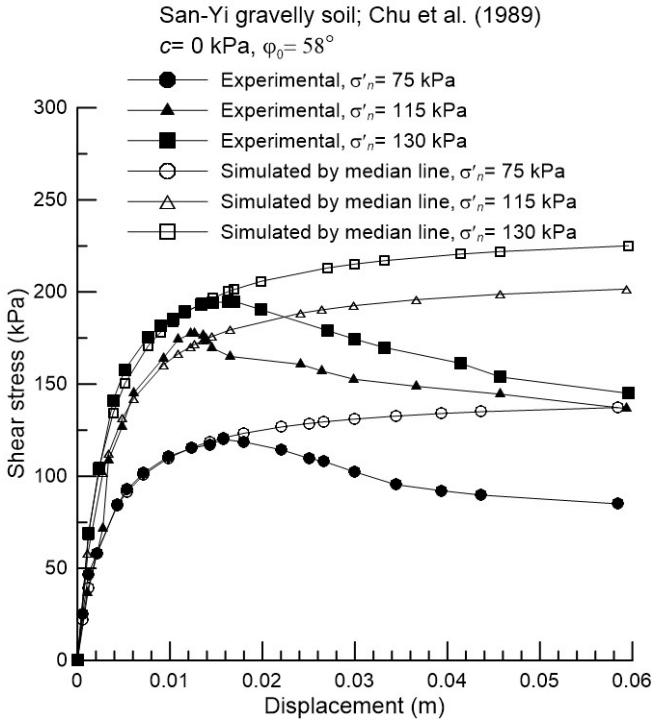

Figure 10.4.2 Comparisons of experimental and simulated stress-displacement curves for San-Yi gravelly soil reported by Chu et al. (1989)

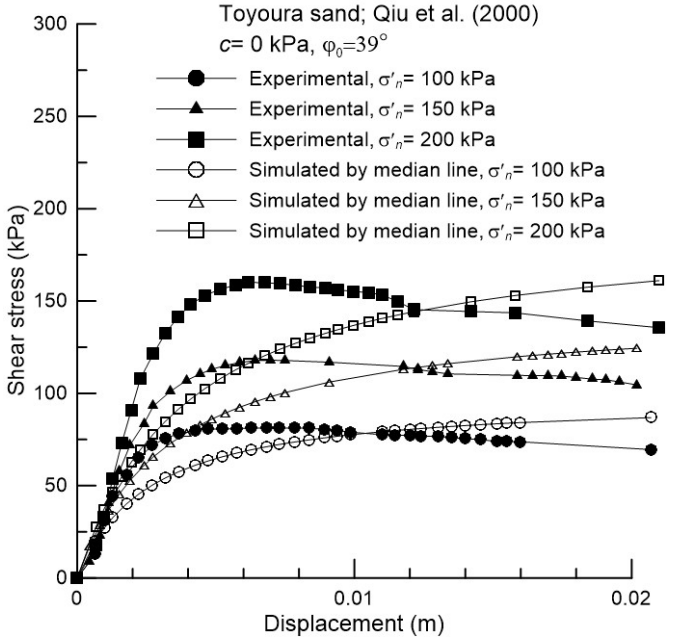

Figure 10.4.3 Comparisons of experimental and simulated stress-displacement curves for Toyoura sand reported by Qiu et al. (2000)

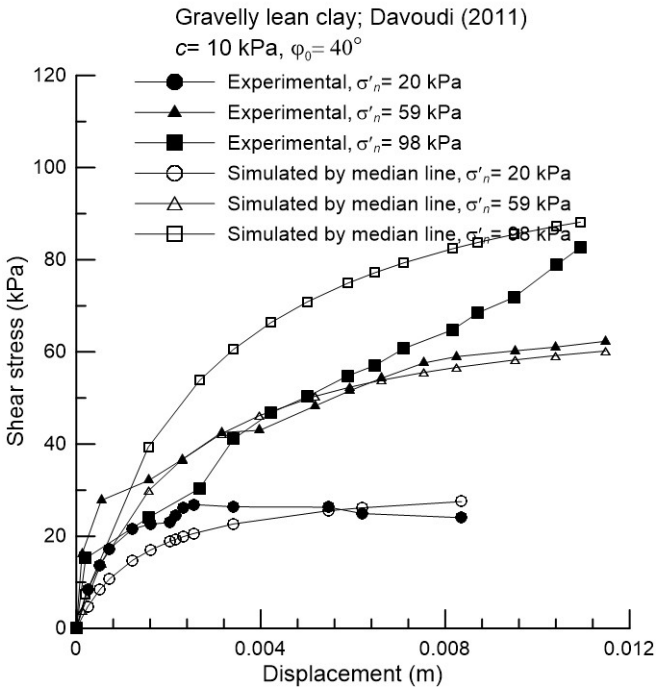

Figure 10.4.4 Comparisons of experimental and simulated stress-displacement curves for gravelly lean clay reported by Davoudi (2011)

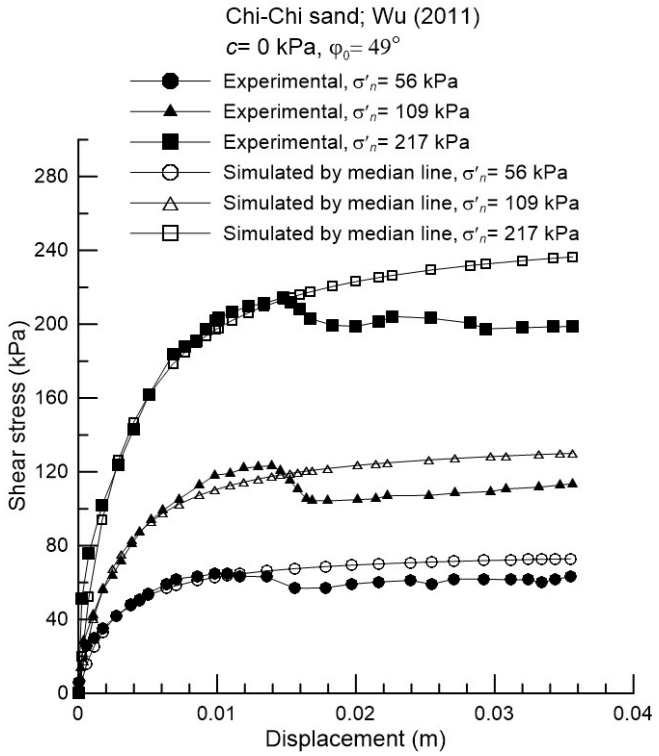

Figure 10.4.5 Comparisons of experimental and simulated stress-displacement curves for Chi-Chi sand reported by Wu (2011)

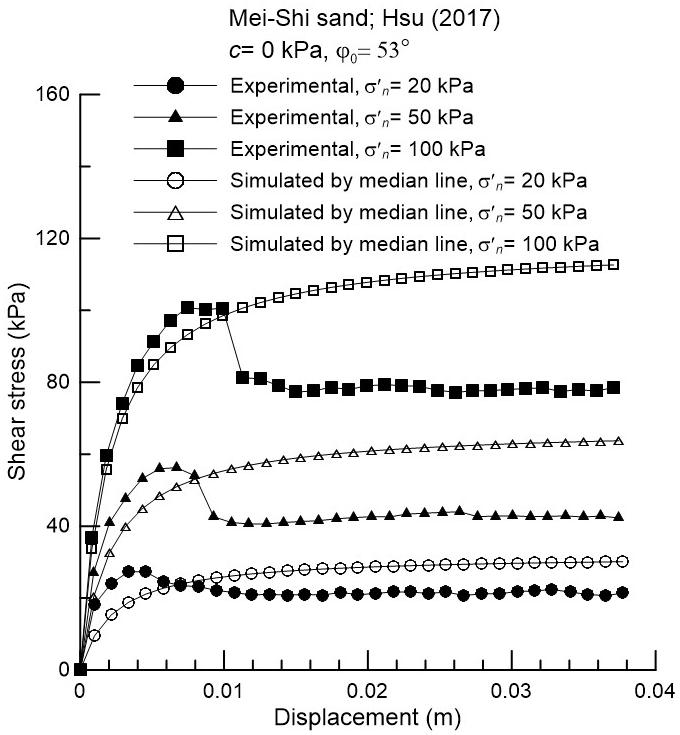

Figure 10.4.6 Comparisons of experimental and simulated stress-displacement curves for Mei-Shi sand reported by Wu (2017)

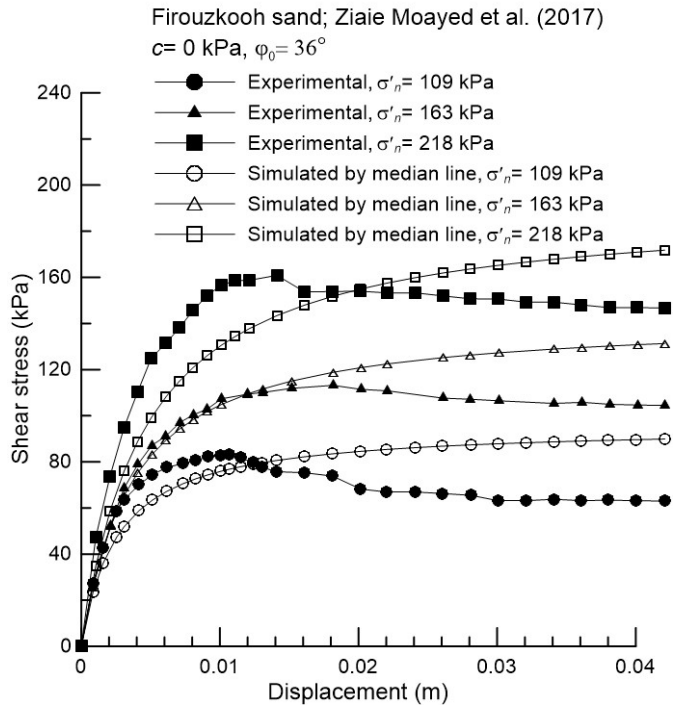

Figure 10.4.7 Comparisons of experimental and simulated stress-displacement curves for Firouzkooh sand reported by Ziaie Moayed et al. (2017)

10.5 GROUNDWATER MODELING IN SLOPE-ffdm 2.0

SLOPE-ffdm 2.0 incorporates five groundwater modeling modes, each designed to simulate specific hydrogeological conditions affecting slope stability and displacement behavior. These modes are embedded in the 'water table' command and are described as follows:

(1) **Piezometric line (Mode 1 of 'water table' command)**:

For a known piezometric line, the porewater pressure (***u***) at any point located a vertical distance **(z)** below the line is calculated based on hydrostatic principles. This condition is illustrated in **Fig. 10.5.1**.

$$u = \gamma_w \cdot z \qquad (10-5-1)$$

γ_w: unit weight of water

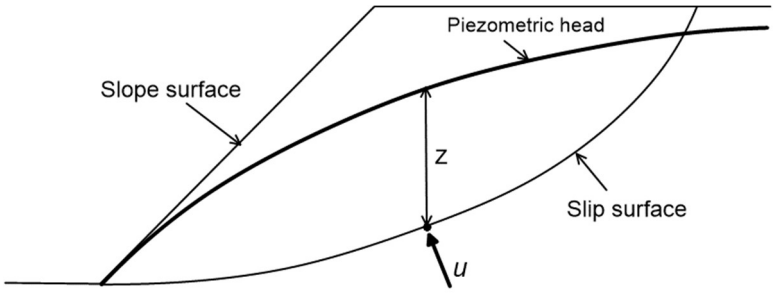

Figure 10.5.1 Porewater pressures along the potential failure surface of a slope with a piezometric line.

(2) Pore pressure ratio (Mode 2 of 'water table' command):

The pore pressure ratio (r_u) has been widely used in geotechnical engineering to account for the excess pore pressure at the completion of a massive soil compaction work, such as the fill dam. The pore pressure at a certain depth (z) from the crest of slope as shown in Fig. 10.5.2:

$$u = r_u \cdot \gamma_m \cdot z \qquad (10-5-2)$$

γ_m: moist unit weight of soil

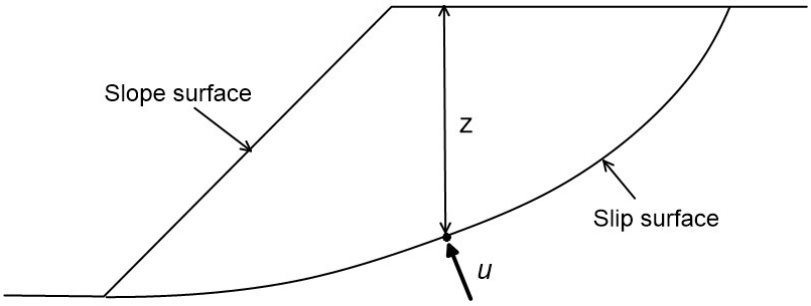

Figure 10.5.2 A saturated slope with a porewater pressure ratio.

(3) Submerged unit weight (Mode 3 of 'water table' command):

Using the submerged unit weight of soils ($\gamma' = \gamma_{sat} - \gamma_w$; γ_{sat}: saturated unit weight of soils; γ_w: unit weight of water) is an alternative way of evaluating the influence of groundwater table in the slope. In this case, the pore pressure (u) at a depth (z) from the crest of the slope is zero, as shown in Fig. 10.5.3:

$$u = 0 \qquad (10-5-3)$$

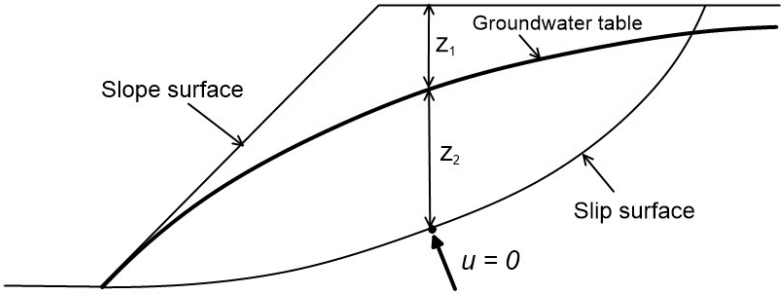

Figure 10.5.3 A potential failure mass with a submerged soil unit weight.

(4) **Hydro-static condition (Mode 4 of 'water table' command)**:

For slopes partially or entirely submerged in static water, hydrostatic pressure acts externally on the slope face, providing lateral support. This condition is modeled as an external load acting on the slope, as depicted in Fig. 10.5.4.

$$u_1 = \gamma_w \cdot z_1 \qquad (10-5-4)$$
$$u_2 = \gamma_w \cdot z_2 \qquad (10-5-5)$$
$$u_3 = \gamma_w \cdot z_3 \qquad (10-5-6)$$
$$u_4 = \gamma_w \cdot z_4 \qquad (10-5-7)$$

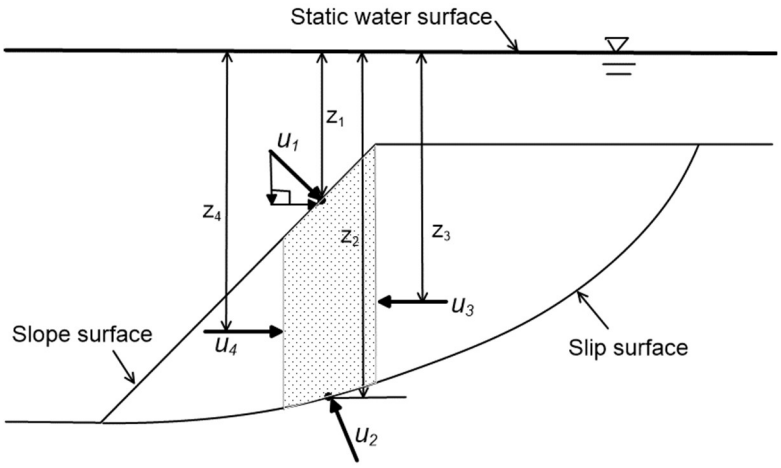

Figure 10.5.4 Porewater pressures for a slice in a slope submerged in water.

(5) Phreatic line (Mode 5 of 'water table' command):

A phreatic line can be horizontal - representing hydrostatic equilibrium - or curved, reflecting seepage flow. In this mode, a simplified flow net is assumed with straight streamlines and equipotential lines. The pore pressure at depth z below the phreatic surface is estimated using this framework.

$$u = \gamma_w \cdot z \cdot \cos^2 \theta \qquad (10-5-8)$$

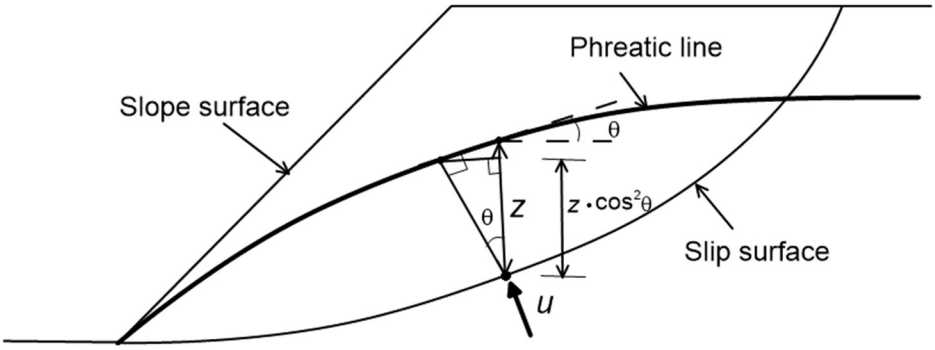

Fig. 2.5.5 Porewater pressures along a potential failure surface of a slope with a phreatic surface

A special case arises when part of the slope is submerged beneath the phreatic line or seepage surface, as illustrated in Fig. 10.5.6. In such cases, the submerged portion is treated as having hydrostatic conditions, consistent with **Mode 4 of the 'water table' command**.

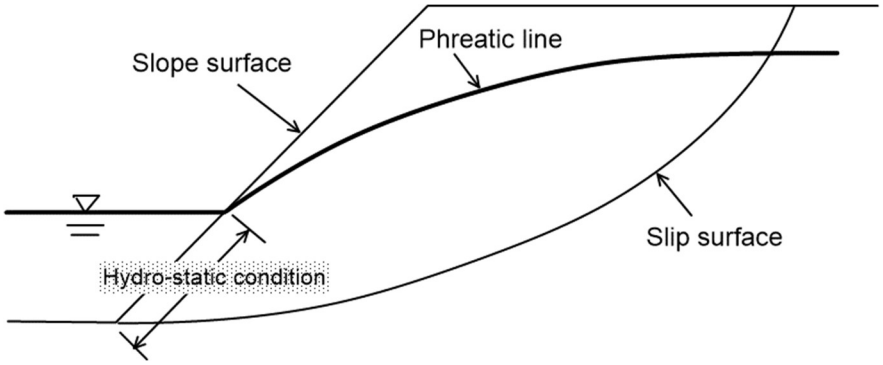

Fig. 10.5.6 A special case of a slope with a phreatic surface and a hydro-static zone

10.6 MODELLING TYPE-1 FACING (GRIVITY FACING)

Type-1 facing is a gravity-type facing with a vertical or a leaning back-face. In the case of a leaning back-face of gravity-type facing (Fig. 10.6.1), only the self-weight of the shaded area is accounted for in the calculation of base reaction and base resistance (R_n and R_b). In addition, a passive resistance in front of the wall, P_p is also considered in the stability analysis. Therefore, an external supporting force, R_b+P_p is considered as a stabilizing force against sliding in stability and displacement analyses. In circular failure analyses, the rotation arms of P_p and R_b are the vertical distances of these forces to the rotation center. In the case of rigorous stability analyses, such as the rigorous Janbu's and Spencer's methods, the location of P_p+R_b is assumed at 1/3 of the wall height.

$$R_b = c_{base} \cdot L_{base} + W' \cdot \tan \varphi_{base} \qquad (10-6-1)$$

$$P_p = 0.5 \cdot K_p \cdot \gamma \cdot D_p^2 + 2c_p\sqrt{K_p} \qquad (10-6-2)$$

$$K_p = tan^2\left(45° + {}^{\varphi_p}/_{2}\right) \qquad (10-6-3)$$

c_{base}, φ_{base}: adhesion and friction angle at the base of wall

L_{base}: base width

W': effective weight of the shaded area of facing

c_p, φ_p: cohesion intercept and internal friction angle of soils in the passive zone

γ: soil unit weight of the passive zone

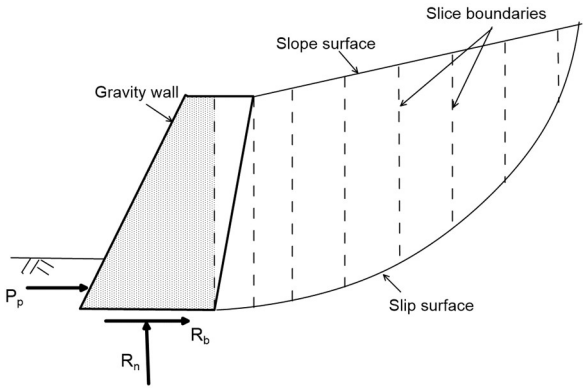

Figure 10.6.1 Self-weight, passive and wall-base resistances of a gravity wall

Note that in all types of analyses (Type-1 through Type-8 analyses), a potential failure surface is not allowed to cut-through the body of gravity facing.

10.7 MODELLING TYPE-2 FACING (MODULAR BLOCK FACING)

The type-2 facing is a modular block facing with a vertical or a leaning back-face as shown in Fig. 10.7.1. In this case, a passing-through-facing failure surface is possible, and the base resistance of the facing column (R_b) is evaluated using the following equation:

$$R_b = c_{inter-block} \cdot L_{inte-bloc} + W' \cdot \tan \varphi_{inter-block} \qquad (10-7-1)$$

$c_{inter\text{-}block}$, $\varphi_{inter\text{-}block}$: adhesion and friction angle at block-block interface

$L_{inter\text{-}block}$: width of facing column.

W': Self-weight of the shaded area of facing column above a certain inter-block face

In the case of passing-through-column-base failure surface, the evaluations of R_n, R_b and P_p are the same with those discussed in Eqs. 10-6-1 through 10-6-3.

10.8 MODELLING TYPE-3 FACING (GABION FACING)

Stability and displacement evaluations for the gabion facing (facing type-3) are identical to the case of modular block facing discussed in Section 10.7.

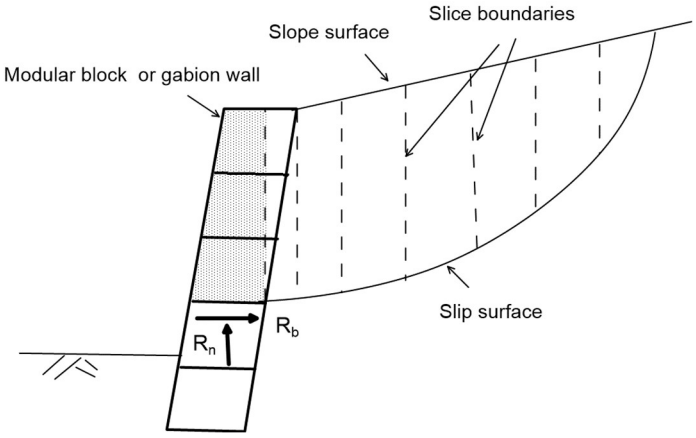

Figure 2.8.1 Self-weight, passive and wall-base resistances of modular block (or gabion) facing

10.9 AUTOMATIC GENERATIONS OF NONCIRCULAR FAILURE SURFACES

Figure 10.9.1 schematically shows a potential failure mass confined by a logarithmic spiral with a rotation center at (x_c,y_c) and radius of r, defined by the following equation:

$$r = r_0 \cdot \exp(\theta \cdot \tan\mu) \qquad (10-8-1)$$

θ : rotation angle (in radian)

For a logarithmic spiral surface passing through two specific points, namely, an upper boundary of (x_1, y_1) and a lower boundary of (x_2, y_2), the value of tan μ which dictates the curvature of the logarithmic spiral can be obtained as:

$$\tan\mu = \frac{ln\frac{r}{r_0}}{\theta} \qquad (10-8-2)$$

In **SLOPE-ffdm 2.0**, the location of rotation center (x_c, y_c) is positioned at:

$$x_c = x_1 \qquad (10-8-3)$$

$$y_c = f_0 \cdot D_m \qquad (10-8-4)$$

D_m: horizontal distance between upper and lower boundaries

f_0: empirical constant (= 0.7)

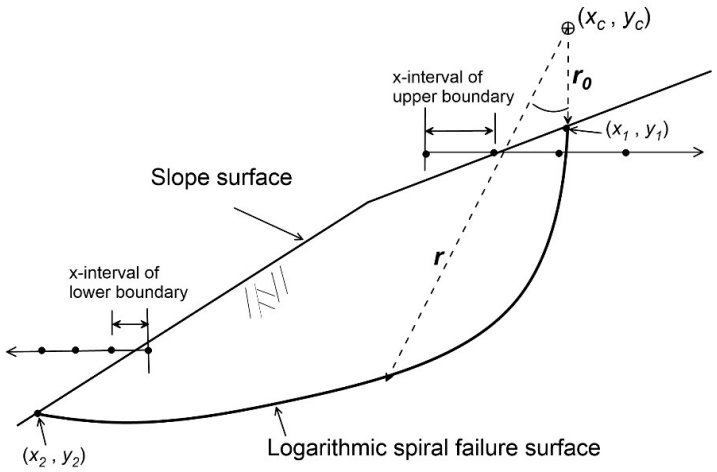

Figure 10.9.1 Geometry of logarithmic spiral failure surface

REFERENCES

Chiang Y.-J. Analyses for rainfall-induced slope displacements taking into account various displacement fields and failure criteria. Master thesis of National Cheng Kung University, Tainan, Taiwan 2017.

Chu, B.-L., Huang, C.-R., Jeng, S.-Y. Study on terrace sedimentary and Tou-ka-san gravelly strata using in-situ direct shear tests. Proceedings of the 3rd National Geotechnical Conference, Taichung City, Taiwan 1989, 695-706.

Davoudi, M.H. Influence of willow root density on shear resistance parameters in fine grain soils using in situ direct shear tests. Res. J. Environ. Sci. 2011, 5, 157-170.

Duncan, J.M. and Chang, C.-Y. Nonlinear analysis of stress and strain in soils" Journal of Soil Mechanics and Foundation Division, Proceedings of ASCE 1970, Vol. 96 (SM5), 1629-1653.

Duncan, J.M. and Wright, S.G. Soil Strength and Slope Stability. John Wiley & Sons, New Jersey, USA, 2005, 295p

Hsu, H.-Y. Modeling on the behavior of soils subjected to cyclic direct shear" Master's thesis, National Cheng Kung University, Tainan, Taiwan, 2017 (In Chinese)

Huang, C.-C. Developing a new slice method for slope displacement analyses. Engineering Geology 2013, Vol. 157, 39-47.

Qiu, J.-Y., Tatsuoka, F., and Uchimura, T. Constant Pressure and Constant Volume Direct Shear Tests on Reinforced Sand. Soils and Foundations 2000, Vol. 40, No. 4, 1-17

Tatsuoka, F., Sakamoto, S., Kawamura, T. and Fukushima, S. (1986) "Strength and deformation characteristics of sand in plane strain compression at extremely low pressures" Soils and Foundations, Vol. 26, No. 1, pp. 65-85.

Wu, K.-W. Applying results of true direct shear tests to the stability analysis for integrated road-dyke structures" Master's thesis, Feng-Chia University, Taichung City, Taiwan, 2011 (In Chinese)

Ziaie Moayed, R., Alibolandi M., and Alizadeh A. Specimen size effects on direct shear test of silty sands, International Journal of Geotechnical Engineering 2017, Vol. 11, No. 2, 198-205.